molecular pharmaceutics

Article

pubs.acs.org/molecularpharmaceutics

Enhancing Targeted Tumor Treatment by Near IR Light-Activatable Photodynamic–Photothermal Synergistic Therapy

Zhen Fan,[†] Xuemei Dai,[†] Yuefeng Lu,[‡] Eugene Yu,[†] Nupur Brahmbatt,[†] NaTasha Carter,[†] Christine Tchouwou,[†] Anant Kumar Singh,[†] Yolanda Jones,[§] Hongtao Yu,[†] and Paresh Chandra Ray*[,†]

[†]Department of Chemistry, Jackson State University, Jackson, Mississippi 39217, United States

[‡]Department of Neurobiology & Anatomical Science, University of Mississippi Medical Center, Jackson, Mississippi 39216, United States

[§]Department of Chemistry, Alcorn State University, Mississippi 39096, United States

ABSTRACT: For several decades, cancer has been one of the most life-threatening diseases. For enhancing anticancer efficiency with minimum side effects, combination therapy is envisioned. The current manuscript reports for the first time the development of a methylene blue (MB) bound nanoplatform, which is capable of delivering targeted diagnostic and combined synergistic photothermal and photodynamic treatment of cancer. Experimental data found that, once the nanoparticle binds with the target cell surface, it can detect LNCaP human prostate cancer cell selectively using fluorescence imaging. Our result shows that the therapeutic actions can be controlled with external NIR light. No cytotoxicity was observed in the absence of NIR light. Targeted photodynamic and photothermal treatment using 785 nm NIR light indicates that the multimodal treatment enhances the possibility of destroying LNCaP prostate cancer cells in vitro dramatically. We discuss the operating principle for the targeted imaging and possible mechanisms for combined therapeutic actions. Our experimental data show that NIR light activated combined therapy for cancer may become a highly effective treatment procedure in clinical settings.

KEYWORDS: *nanoplatform, prostate cancer, selective detection, ROS formation, combined synergistic photothermal–photodynamic therapy*

INTRODUCTION

Recent advances have been achieved with our better understanding of the signaling pathways and molecular underpinnings of cancer drug resistance.[1−4]It has become apparent that a single therapeutic agent shows limited efficiencies in the clinical environment due to the drug-resistance profiles.[5−9] To enhance anticancer efficacy, recent reports indicate that multimodal therapy can be a highly promising strategy with minimum side effects.[10−19] In the past few years, several articles have demonstrated that combined therapy using multifunctional nanoparticles may be better designs for cooperatively suppressing cancer development.[16−24] The design of multifunctional nanoparticles for diagnostic, therapeutic, and theranostic agents for a wide variety of human diseases can have a revolutionary impact on the pharmaceutical industry, as reported in the past decade.[24−34] Since multiple functions are integrated into a single nanostructure, the nanoplatform can be used for image-guided combined therapy.[35−45] In the past decade, several different types of therapeutic approaches have been developed for cancer treatment.[1−9] Among all those, photodynamic therapy (PDT) and photothermal therapy (PTT) involving near-infrared (NIR) light have been shown to possess unique advantages, including remote controllability and low systemic toxicity and side effects.[3−13] Our groups and other groups have shown that magnetic core–plasmonic shell nanoparticle can be used for imaging and photothermal therapy of cancer cell.[8,25,28,37] Since the combination of therapeutic approaches may cooperatively suppress cancer development with potential advantages of synergistic effects and reversal of drug resistance, the current manuscript reports, for the first time, methylene blue (MB) bound magnetic core–plasmonic shell nanoplatform based cell imaging and combined photodynamic and photothermal synergistic targeted therapy of cancer. Our result shows that the cancer cells can be selectively separated, imaged, and destroyed significantly by illumination with 785 nm near IR continuum light for a few minutes. Experimental data demonstrated that, due to the synergistic effect, the therapeutic efficacy of the nanoplatform was enhanced significantly compared to PDT or PTT alone. Since the clinically ideal phototherapeutic biological window for cancer is between 700 and 1100 nm,[2−10] and also the nanoplatform has strong absorption at 785 nm, we have

Received: May 14, 2013
Revised: January 22, 2014
Accepted: February 25, 2014
Published: February 25, 2014

reported 785 nm near IR light triggered combined synergistic therapy for tumor.

Methylene blue is a well-known photodynamic therapy drug.[46−49] In the past few decades, PDT has been known to be a minimally invasive technique for clinical cancer therapy, where light-activated photosensitizers generate reactive oxygen species, which can irreversibly damage cancerous cells and tissues.[8−14,46−49] Since methylene blue does not have enough absorption at 785 nm, where light penetration can be a few centimeters through tissue surface, it cannot be used for near IR therapeutic treatment. The poor selectivity of methylene blue for the targeted tumor sites minimizes PDT efficacy in vivo and also increases the potential phototoxicity to normal tissues. To improve these disadvantages and for the near-infrared light based deep tissue treatment, we have used MB-bound nanoplatform which has a strong absorption at 785 nm light, as shown in Figure 1. As shown in Scheme 1, in our design, we

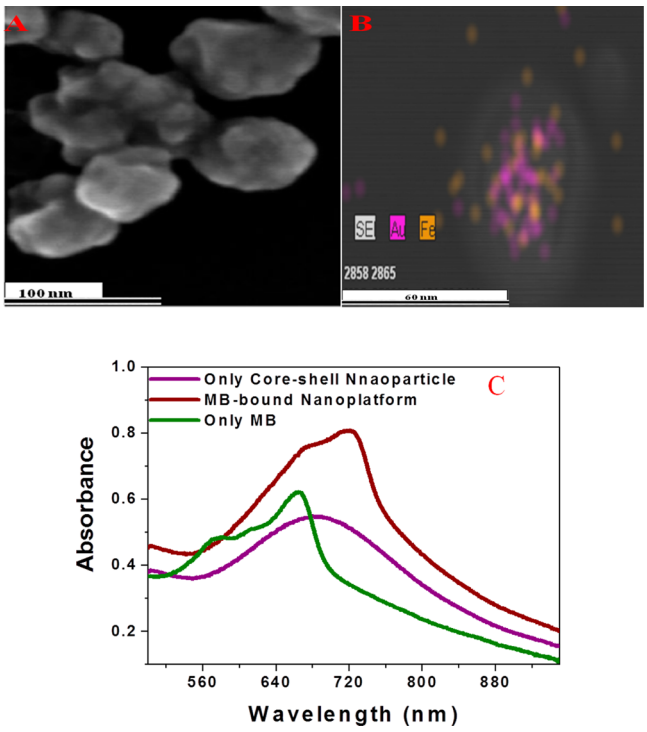

Figure 1. (A) SEM images of freshly prepared core−shell plasmonic nanopopcorn. (B) EDX mapping shows the presence of Fe and Au in a core−shell nanoparticle. (C) Absorption spectra of core−shell nanoparticle, methylene blue, and methylene blue conjugated nanoplatform. The strong long wavelength band in the near IR region (λ_{max} = 740 nm) for the nanoplatform is due to the oscillation of the conduction band electrons of gold.

have used methylene blue as a photodynamic therapy drug and as a fluorescence imaging probe. On the other hand, gold shell in our design core−shell nanoparticle has been used as an optical "nano heater" for IR light induced photothermal killing of cancer cells, where the plasmonic shell absorbs 785 nm light and converts it into cytotoxic heat via electron−phonon relaxation.[20−38] In this manuscript, we have shown that MB-bound nanoplatform can be used for simultaneous delivery of optical diagnostic and multimodal synergistic treatment of cancer diseases. We have demonstrated that, in the nanoplatform, the magnetic core is capable of rare tumor cell isolation and enrichment using a small bar magnet. In our design, the MB-modified A9 aptamers are attached to a nanoplatform through −SH linkage for (a) specific LNCaP prostate cancer cell recognition via the A9 aptamers;[40] (b) fluorescence imaging using the MB fluorescence probe; and (c) targeted synergistic combined PDT and PTT therapy. To make sure that the combined therapy using the nanoplatform delivers only to the malignant cells, we have demonstrated that, in our design, combined therapy is only activated in the presence of NIR light and no toxicity was observed without light exposure.

RESULTS AND DISCUSSION

Nanoplatforms which can be used for selective imaging and combined therapy were developed via a several step process, as described in the Experimental Section. At first, popcorn shape iron magnetic core−gold shell nanoparticles were prepared using our reported method.[15]Next, Hitachi 5500 ultrahigh-resolution SEM microscope and UV−visible absorption spectrum were used to characterize the iron core−magnetic shell nanoparticles, as shown in Figure 1A,B. The absorption spectrum, reported in Figure 1C, clearly shows the plasmon band around 740 nm, which indicates the formation of gold shell in the core−shell nanoparticle. The SEM image, as reported in Figure 1A, shows a clear small spike, which indicates the formation of popcorn shape core−shell nanoparticle. Figure 1B shows the energy dispersion X-ray (EDX) data, which clearly demonstrate the presence of iron and gold in the core−shell nanoparticle. To find out whether the nanoplatform developed by us can be used for combined synergistic therapeutic action for cancer, we have used the LNCaP human prostate cancer cell line, which is well-known to overexpresses the prostate specific membrane antigen (PSMA) on the cell surface. For targeted imaging and synergistic therapy, we have modified the nanoplatform with MB-bound A9 RNA aptamer, which is known to be specific to PSMA.[40] For this purpose, initially, the core−shell nanoparticle was coated with thiolated polyethylene glycol (HS-PEG),which helps to avoid nonspecific interactions with cells and cell media. After PEGylation, thiol-modified MB-bound A9 aptamers were attached via Au−S chemistry. Next to show the capability of our nanoplatform to separate cancer cells from normal cells, *LNCaP* cancer cell suspension containing 10^3 cells/mL was mixed with 1 mL of PSMA-negative human skin HaCaT cell suspension containing 10^7 cells/mL. After that we added 100 μL of nanoplatform to the cell mixture and incubated for 120 min under gentle shaking. Next, to separate nanoplatform attached cancer cells from the mixture, we used a bar. At the end, after magnetic separation, we used fluorescence image, TEM, and enzyme-linked immunosorbent assay kits for the characterization of cells that bind with nanoplatform and separated them by bar magnet. Similarly, cells that did not bind with the nanoplatform were also characterized using microscopic and optical imaging technique as well as using enzyme-linked immunosorbent assay.

Our enzyme-linked immunosorbent assay results indicate no PSMA presence in the fractions of cell suspensions that did not bind to the nanoplatform, which indicates the absence of LNCaP cells in cell suspension which are not separated by the magnet. On the other hand, we find that PSMA was present in the nanoplatform attached cell suspension. Enzyme-linked immunosorbent assays results clearly indicate that LNCaP cells are attached to the nanoplatform. From the enzyme-linked immunosorbent assay experiments we have estimated that the LNCaP cancer cell recovery by bar magnet was about 97%. Our

Scheme 1. Schematic Representation Showing Working Principle of Combined Synergistic Action Using Photodynamic and Photothermal Therapy

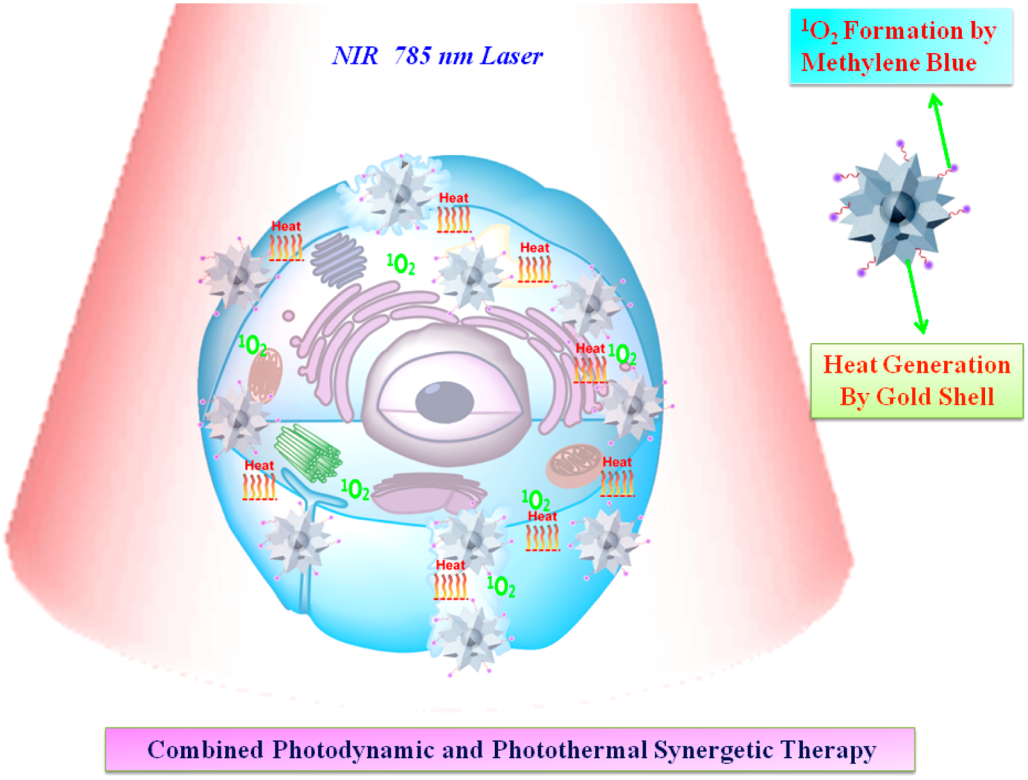

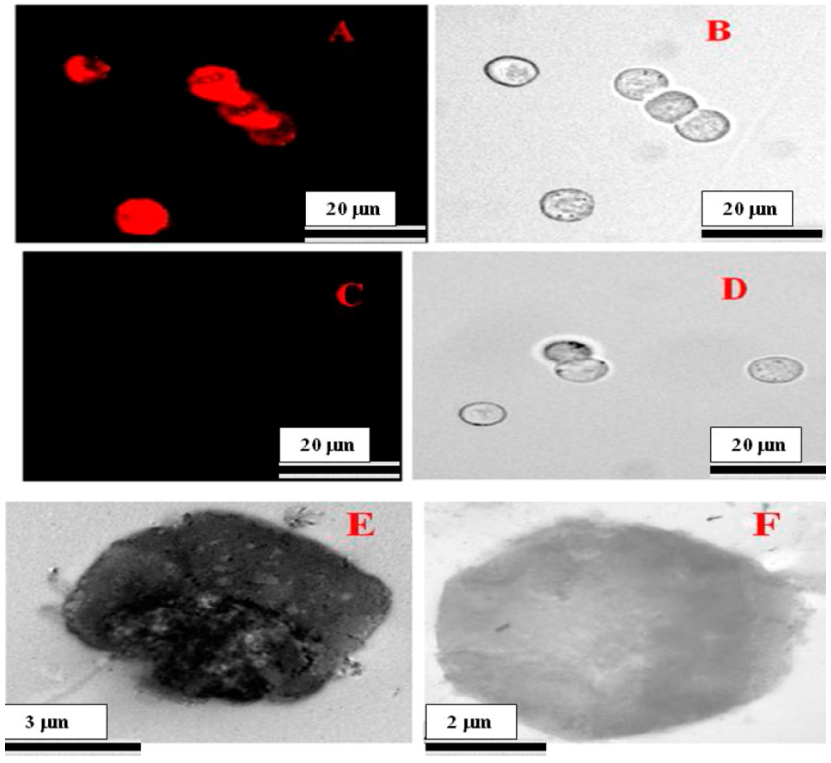

Figure 2. (A) Fluorescent images of nanoplatform-attached LNCaP human prostate cancer cells, after LNCaP cells were separated from cell mixture using a magnet. (B) Bright-field image of the same LNCaP cells after magnetic separation. (C) Fluorescent images of cell suspension which are not separated by the magnet. (D) Bright-field image of cell suspension which are not separated by the magnet. For fluorescence imaging, we used 650 nm excitation and the fluorescence was collected between 680 and 720 nm. (E) TEM image of nanoplatform attached LNCaP cells after magnetic separation. (F) TEM image of suspension of cells which are not separated by the magnet, which is mostly HaCaT cells.

dx.doi.org/10.1021/mp4002816 | *Mol. Pharmaceutics* 2014, 11, 1109−1116

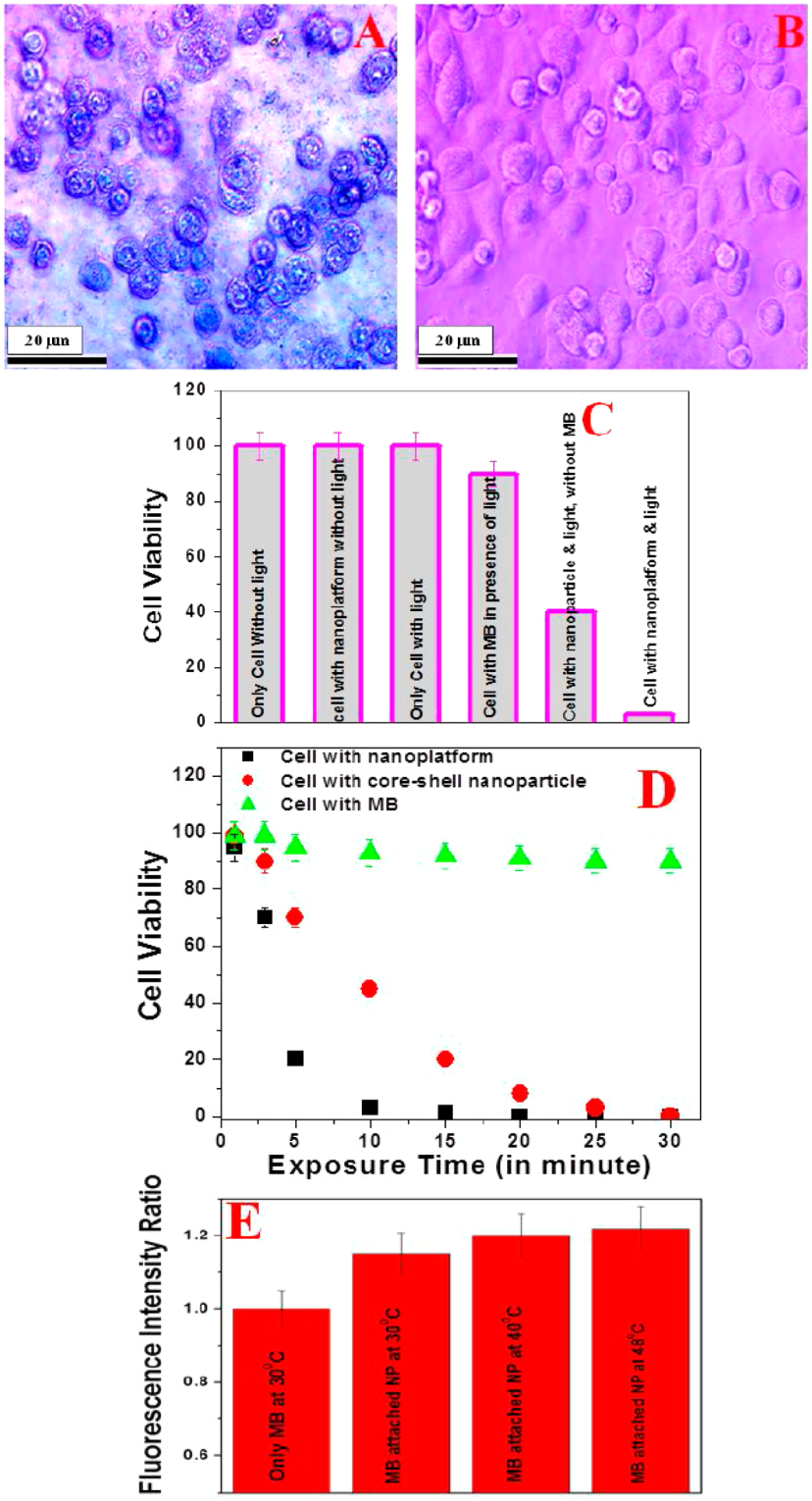

Figure 3. (A) Bright-field inverted microscopic images of MB-bound nanoplatform attached LNCaP prostate cancer cells, after being separated by a magnet and followed by irradiation with 785 nm near IR light at 1 W/cm^2 for 7 min. For imaging we used 485 nm excitation, and the fluorescence was collected between 520 and 535 nm. The bright-field image clearly shows that cancer cells are dead after combined therapy. (B) Bright-field inverted microscopic images of prostate cancer LNCaP cells in the absence of nanoplatforms or MB and irradiated with 785 nm light at 1 W/cm^2 for 20 min followed by staining with trypan blue. The bright-field image clearly shows that cancer cells are alive after 785 nm light exposure in the absence of nanoplatforms or MB. (C) Plot showing the percentage of cell viability in MB-bound nanoplatform attached LNCaP cells in the absence of laser light and in the presence of laser light. Plot shows no cytotoxicity in the absence of NIR light. It also shows dramatic synergistic action in the case of combined therapy. (D) Plot showing time-dependent LNCaP prostate cancer cell viability after irradiation with 785 nm near IR light at 1−2 W/cm^2 for 35 min, in the case of PDT, PTT, and combination therapy. Data clearly shows a synergistic therapeutic effect for prostate cancer treatment in the case of combined therapy. (E) Plot showing how ROS formation from MB can vary in the presence of core−shell nanoparticles at different temperatures.

dx.doi.org/10.1021/mp4002816 | *Mol. Pharmaceutics* 2014, 11, 1109−1116

fluorescence imaging data using confocal fluorescence microscope, as shown in Figure 2A−D, clearly shows that the nanoplatform was bound only to LNCaP cells and not HaCaT cells. Similarly, TEM images (Figure 2E,F) indicate that the nanoplatform attached only to LNCaP cells and not normal HaCaT cells. All the experimental results, described above, clearly indicate that the MB-bound A9-aptamer-conjugated nanoplatform developed by us is highly selective for binding with the LNCaP prostate cancer cell line, which overexpresses PSMA.

Next, to find out whether our design of core−shell nanoplatform can be used for multimodal therapy, after successful targeted prostate cancer LNCaP cell separation, we performed NIR irradiation experiments using 785 nm excitation light. For this purpose, at first, we performed a cytotoxicity experiment in the absence of NIR light to determine whether the nanoplatform developed by us is cytotoxic or not. Next, to determine if the combined therapy is much superior to single therapy, we designed several different experiments, which we discuss now. For the cytotoxicity measurement, MB-bound nanoplatform attached LNCaP cells were incubated for 12 h without any laser light. Our experimental data, as shown in Figure 3C, clearly shows that no cell death was observed even after 12 h of incubation, which indicates that the nanoplatform developed by us is not cytotoxic in the absence of external NIR light.

On the other hand, as shown in Figure 3, NIR light induced experimental data clearly shows that 97% of cells were dead, when MB-bound nanoplatform attached LNCaP cells were irradiated with 785 nm light at 1 W/cm^2 power for 10 min. The above data clearly indicate that our nanoplatform can only be activated for combined therapy in the presence of near IR 785 nm light and also the MB-bound nanoplatform is not cytotoxic in the absence of external NIR light. To determine the amount of cell death due to the combined therapy in the presence of 785 nm light, we used the typan blue test to find the amount of dead cells. Similarly, we used the MTT test to determine the number of live cells during the combined photodestruction process. Bright-field inverted microscope image data, as shown in Figure 3A, clearly show that LNCaP cancer cells were deformed during the combined therapy process. The cell death following nanoplatform exposure to 785 nm NIR light could be due to numerous factors, including ROS induced cancer cell death due to the presence of MB and thermal disintegration by gold shell nanoparticles.[25−40] Figure 3B shows the bright-field inverted microscope images of LNCaP cells in the absence of nanoplatform and MB, after 20 min of exposure by 785 nm light. Bright-field image and MTT test data, as shown in Figure 3, clearly show no cell death in the absence of a nanoplatform, which indicates that our nanoplatform based combined therapeutic killing is highly selective for the LNCaP cancer cells which were only attached to the nanoplatform. Next, to understand how the temperature varies during the NIR radiation based combined therapy process, we used a MikroShot camera to measure thermal imaging at 1 min intervals. Our thermal imaging experiment indicated that the temperature increased to about 48 °C when MB-bound A9-aptamer-attached nanoplatforms with LNCaP cancer cells were exposed to 785 nm laser light at 1 W/cm^2 power. We also noted that the temperature increased to only 30 °C for LNCaP cells in the absence of a nanoplatform, under the same light exposure conditions. It is exciting to note from our experimental data, as shown in Figures 3C and 3D, that when the two treatments were combined under a single 785 nm NIR light irradiation, the LNCaP prostate cancer cell viability was remarkably reduced. Cell viability was much lower in the case of PDT and PTT combined therapy than that by the individual ones. This clearly shows that, by using MB-bound nanoplatform, we can very easily achieve synergistic therapeutic effects for prostate cancer treatment.

To determine the amount of LNCaP cancer cell death due to the 785 nm light induced photothermal killing effect, A9-aptamer-bound core−shell nanoparticle without MB was attached to LNCaP cells and then cells were irradiated with 785 nm near IR light at 1 W/cm^2 power at different time intervals. For direct comparison between combined therapy and single therapy, we kept the A9-aptamer-bound core−shell nanoparticles and LNCaP cell concentration the same as in the case of photothermal killing and combined therapy. The time interval data, as shown in Figure 3D, show that it takes about 25 min of PTT experiment to kill most of the LNCaP prostate cancer cells, whereas it takes only 10 min to kill the same amount of LNCaP prostate cancer cells using combined therapy.

Next, to estimate the amount of cell death due to the photodynamic therapy only, we incubated MB with LNCaP cells for 30 min, and then cells were irradiated with 785 nm near IR light at 1 W/cm^2 power at different time intervals. We kept the MB and LNCaP cell concentration the same in the case of the photodynamic and combined therapy process. As shown in Figure 3D, even after 25 min of photodynamic therapy only 10% of the cells were dead. And this is mainly due to the fact that MB does not have enough absorption at 785 nm light, as shown in Figure 1C. By combining all the experimental data, one can see a significant synergistic therapeutic effect. In MB-bound A9-aptamer-attached nanoplatform, MB utilizes his ability to form reactive oxygen species in the presence of light, to kill LNCaP prostate cancer cells. So the efficiency of photodynamic killing by nanoplatform is highly dependent on the formation of ROS capability by MB. Recently we and other groups have reported that ROS formation by PDT dye using near IR light can be enhanced in the presence of gold nanoparticles.[9,15] Next, to understand the synergistic combined therapy mechanism for destroying LNCaP prostate cancer cells, we measured the cellular ROS formation during the PDT process using singlet oxygen sensor green reagent (SOSG, Sigma). For this purpose, during the PDT process, the fluorescence intensity was measured using the microplate reader with the excitation wavelength at 485 nm and the emission wavelength at 528 nm and MB was used as the standard material for normalization process. Our experimental results, as shown in Figure 3E, clearly show the elevated ROS formation in the presence of core−shell nanoparticle at different temperatures. This increment can be due to the fact that, as shown in Figure 1E, methylene blue absorption at 670 nm enhances in the presence of core−shell nanoparticles. This enhancement can be attributed to the presence of high localized plasmonic field on the surface of nanoparticles. Our experimental data, as shown in Figure 3E, show that ROS formation by MB can be expected to be more efficient as the temperature increases during the phtothermal therapy process. Our experimental result proves that the combined PDT and PTT treatment regime can dramatically enhance the possibility of destroying LNCaP prostate tumor cells in vitro due to the synergistic therapeutic effect combined with the formation of

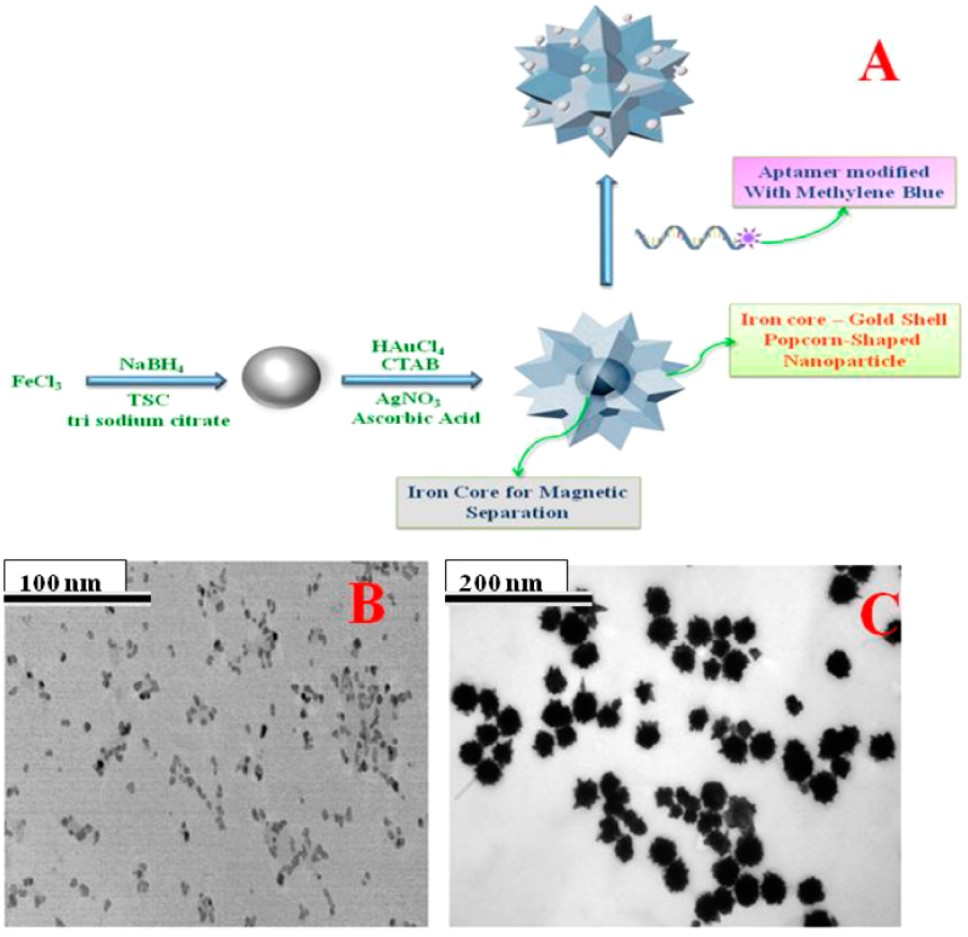

Figure 4. (A) Schematic representation showing the synthesis of methylene blue (MB) attached nanoplatform. (B) TEM image of freshly prepared iron nanoparticle. (C) TEM image of freshly prepared magnetic core–plasmonic shell gold nanopopcorn.

more ROS during PTT, due to the presence of plasmonic nanoparticle surface and elevated temperature.

CONCLUSION

In conclusion, in this article we have reported the development of a methylene blue bound nanoplatform which can deliver targeted diagnostic and combined synergistic photothermal and photodynamic treatment of cancer cells. We found that the MB-bound A9-aptamer-attached nanoplatform is highly selective for binding to PSMA positive LNCaP prostate cancer cells. We have shown that, in the absence of NIR light, no cytotoxicity has been observed, whereas the nanoplatform can be used for 785 nm NIR light activated combined PTT and PDT therapy. Our experimental data using 785 nm NIR light excitation show that a synergistic therapeutic effect can be obtained using multimodal treatment. Our experimental data show that combined PDT and PTT can dramatically enhance the killing LNCaP prostate cancer cells in vitro, which indicates that the multimodal therapeutic material reported by us may become a more effective system for cancer therapy. Nanoplatform materials developed by us also have the capability to lower the MB's negative effect as a PDT dye in the unnecessary nontargeted area. Though we are in a relatively early stage of development of nanoplatform based synergistic combined therapy of tumor, we believe that the reported assay can have enormous potential for rapid early stage circulating tumor cell detection and combined therapeutic destruction of cancer, once it is optimized properly in the clinical environment.

EXPERIMENTAL SECTION

Materials. All chemicals, including sodium borohydride, $FeCl_3$, $HAuCl_4 \cdot 3H_2O$, and sodium citrate, were purchased from Sigma-Aldrich and Fisher Scientific. We obtained LNCaP cells, growth media to grow cancer cells, phosphate buffered saline, trypsin, and fetal bovine serum from the American Type Culture Collection (ATCC, Rockville, MD).

Synthesis of MB-Bound Nanoplatforms. We synthesized the MB-bound nanoplatform through a several step process, as shown in Figure 4A. At first, 15 nm size iron nanoparticles were synthesized using our reported method,[14,37] as shown in Figure 4B. Next, popcorn shaped iron magnetic core–gold shell nanoparticles were synthesized in the presence of $HAuCl_4$ and CTAB using our reported method.[14,37] After that magnetic core–plasmonic shell nanoparticles were separated by magnet and washed by water and ethanol. Core–shell nanoparticles were characterized using a JEM-2100F transmission electron microscope (TEM) and UV–visible absorption spectrum, as reported in Figures 1A,B and 4B,C. In the next step, methylene blue attachment was performed via A9 RNA aptamer which is specific to PSMA.[40] For this purpose, initially, the nanoplatform was coated by thiolated polyethylene glycol (HS-PEG). After that thiol-modified MB-bound A9 aptamers were attached via Au–S chemistry, using our reported method.[37] Using

fluorescence analyses after the addition of potassium cyanide, we determined that there were about 150−200 aptamers per synergistic combined therapeutic nanoplatform.

Cell Culture and Incubation with Nanoplatforms. LNCaP human prostate cancer cells were grown according to the ATCC procedure as we have reported before.[28,30,37] Using enzyme-linked immunosorbent assay kit we found out that the amount of PSMA in LNCaP cells was 7.9×10^6/cell. No PSMA was found in HaCaT cells. For binding nanoplatforms with cancer cells, initially, different numbers of LNCaP prostate cancer cells were immersed into the MB-bound nanoplatforms at room temperature for 120 min. After that we used a bar magnet for the magnetic separation experiment. After magnetic separation, we performed TEM, SEM, and fluorescence analyses (as shown in Figures 2 and 4). Using enzyme-linked immunosorbent assays, we estimated that there were about 100−120 attached nanoplatforms/cell.

Fluorescence Analysis. For fluorescence imaging, we used 650 nm excitation light from an Olympus IX71 inverted confocal fluorescence microscope. The microscope was fitted with a SPOT Insight digital camera for fluorescence imaging.

Photothermal and Photodynamic Combined Destruction of LNCaP Prostate Cancer Cells and Determination of the Percentage of Live Cells. For the combined destruction or single model destruction experiments, we have used a continuous-wavelength OEM laser operating at 785 nm at 2 W/cm^2 power for 10−25 min. For finding the amount of cell death, we used MTT (ATCC CA# 30-1010k) and typan blue test, using our reported method.[28,30,37]

ROS Generation Measurement. For the measurement of cellular ROS formation during combined and single treatment, we have used singlet oxygen sensor green reagent (SOSG, Sigma) and followed the manufacturer's protocol. For this purpose we used 485 nm as excitation wavelength. The fluorescence intensity at 528 nm was measured using the microplate reader.

AUTHOR INFORMATION

Corresponding Author

*E-mail: paresh.c.ray@jsums.edu. Fax: 601-979-3674.

Notes

The authors declare no competing financial interest.

ACKNOWLEDGMENTS

P.C.R. is grateful for NSF-PREM Grant No. DMR-1205194 and NSF-REU Grant No. 1156111 for their generous funding for nanomaterial research. N.C. thanks NIH-MARC program Grant No. 5-T34-GM007672-28 for her fellowship. We also thank NIH-RCMI Grant. No. 5G12RR013459 for core facilities.

REFERENCES

(1) Cancer Nanotechnology Plan, NIH Publication No. 11-7794, 2010.

(2) Zamboni, W. C.; Torchilin, V.; Patri, A. K.; Hrkach, J.; Stern, S.; et al. Best, Practices in Cancer Nanotechnology: Perspective from NCI Nanotechnology Alliance. *Clin. Cancer Res.* **2012**, *18*, 3229−3241.

(3) Dreaden, E. C.; Mackey, M. A.; Huang, X.; Kang, B.; El-Sayed, M. A. Beating Cancer in Multiple Ways Using Nanogold. *Chem. Soc. Rev.* **2011**, *40*, 3391−3404.

(4) Lovell, J. F.; Liu, W. B. T.; Chen, J.; Zheng, G. Activatable Photosensitizers for Imaging and Therapy. *Chem. Rev.* **2010**, *110*, 2839−2857.

(5) Cabral, H.; Nishiyama, N.; Kataoka, K. Supramolecular nanodevices: Fom design validation to theranostic nanomedicine. *Acc. Chem. Res.* **2011**, *44*, 999−1008.

(6) Saha, K.; Agasti, S. S.; Kim, C.; Li, X.; Rotello, V. M. Gold Nanoparticles in Chemical and Biological Sensing. *Chem. Rev.* **2012**, *112*, 2739−2779.

(7) Ganta, S.; Amij, i M. Coadministration of Paclitaxel and Curcumin in Nanoemulsion Formulations To Overcome Multidrug Resistance in Tumor Cells. *Mol. Pharmaceutics* **2009**, *6*, 928−939.

(8) Lal, S.; Clare, S. E.; Halas, N. J. Nanoshell-Enabled Photothermal Cancer Therapy: Impending Clinical Impact. *Acc. Chem. Res.* **2008**, *41*, 1842−1851.

(9) Wang, J.; Zhu, G.; You, M.; Song, E.; Shukoor, M. I.; Zhang, K.; Altman, M. B.; Chen, Y.; Zhu, Z.; Huang, C. Z.; et al. Assembly of Aptamer Switch Probes and Photosensitizer on Gold Nanorods for Targeted Photothermal and Photodynamic Cancer Therapy. *ACS Nano* **2012**, *6*, 5070−5077.

(10) Zhang, M.; Murakami, T.; Ajima, K.; Tsuchida, K.; Sandanayaka, A. S.; Ito, O.; Iijima, S.; Yudasaka, M. Fabrication of ZnPc/protein nanohorns for double photodynamic and hyperthermic cancer phototherapy. *Proc. Natl. Acad. Sci. U.S.A.* **2008**, *105*, 14773−14778.

(11) Misra, R.; Sahoo, S. K. Coformulation of Doxorubicin and Curcumin in Poly(D,L-lactide-*co*-glycolide) Nanoparticles Suppresses the Development of Multidrug Resistance in K562 Cells. *Mol. Pharmaceutics* **2011**, *8*, 852−866.

(12) Zahedi, P.; Souza, R. D.; Huynh, L.; Piquette-Miller, M.; Allen, C. Combination Drug Delivery Strategy for the Treatment of Multidrug Resistant Ovarian Cancer. *Mol. Pharmaceutics* **2011**, *8*, 260−269.

(13) Sanson, C.; Diou, O.; Thévenot, J.; Ibarboure, E.; Soum, A.; Brûlet, A.; Miraux, S.; Thiaudière, E.; Tan, S.; Brisson, A.; Dupuis, V.; Sandre, O.; Lecommandoux, S. Doxorubicin loaded magnetic polymersomes: Theranostic nanocarriers for MR imaging and magneto-chemotherapy. *ACS Nano* **2011**, *5*, 1122−1140.

(14) Fan, Z.; Senapati, D.; Khan, S. A.; Singh, A. K.; Hamme, A.; Yust, B.; Sardar, D.; Ray, P. C. Popcorn-Shaped Magnetic Core−Plasmonic Shell Multifunctional Nanoparticles for the Targeted Magnetic Separation and Enrichment, Label-Free SERS Imaging, and Photothermal Destruction of Multidrug-Resistant Bacteria. *Chem.—Eur. J.* **2013**, *19*, 2839−2847.

(15) Dai, X.; Fan, Z.; Lu, Y.; Ray, P. C. Multifunctional Nanoplatforms For Targeted MDRB Theranostic Applications. *ACS Appl. Mater. Sci.* **2013**, *5*, 11348−11354.

(16) Wang, Y.; Wang, K.; Zhao, J.; Liu, X.; Bu, J.; Yan, X.; Huang, R. Multifunctional Mesoporous Silica-Coated Graphene Nanosheet Used for Chemo-photothermal Synergistic Targeted Therapy of Glioma. *J. Am. Chem. Soc.* **2013**, *135*, 4799−4804.

(17) Yu, J.; Javier, D.; Yaseen, M. A.; Nitin, N.; Richards-Kortum, R.; Anvari, B.; Wong, M. S. Self-assembly synthesis, tumor cell targeting, and photothermal capabilities of antibody-coated indocyanine green nanocapsules. *J. Am. Chem. Soc.* **2010**, *132*, 1929−1938.

(18) Lin, J.; Wang, S.; Huang, P.; Wang, Z.; Chen, S.; Niu, G.; Li, W.; He, J.; Cui, D.; Lu, G.; Chen, X.; Nie, Z. Photosensitizer-Loaded Gold Vesicles with Strong Plasmonic Coupling Effect for Imaging-Guided Photothermal/Photodynamic Therapy. *ACS Nano* **2013**, *7*, 5320−5329.

(19) Greco, F.; Vicent, M. J. Combination Therapy: Opportunities and Challenges for Polymer-Drug Conjugates as Anticancer Nanomedicines. *Adv. Drug Delivery Rev.* **2009**, *61*, 1203−1213.

(20) Al-Lazikani, B.; Banerji, U.; Workman, P. Combinatorial Drug Therapy for Cancer in the Post-Genomic Era. *Nat. Biotechnol.* **2012**, *30*, 1−13.

(21) Peer, D.; Karp, J. M.; Hong, S.; Farokhzad, O. C.; Margalit, R.; Langer, R. Nanocarriers as an emerging platform for cancer therapy. *Nat. Nanotechnol.* **2007**, *2*, 751−760.

(22) Liu, H. Y.; Chen, D.; Li, L. L.; Liu, T. L.; Tan, L. F.; Wu, X. L.; Tang, F. Q. Multifunctional Gold Nanoshells on Silica Nanorattles: a Platform for the Combination of Photothermal Therapy and

Chemotherapy with Low Systemic Toxicity. *Angew. Chem., Int. Ed.* **2011**, *50*, 891−895.
(23) Park, J. H.; Maltzahn, G. V.; Ong, L. L.; Centrone, A.; Hatton, T. A.; Ruoslahti, E.; Bhatia, S. N.; Sailor, M. J. Cooperative Nanoparticles for Tumor Detection and Photothermally Triggered Drug Delivery. *Adv. Mater.* **2010**, *22*, 880−885.
(24) Wang, S.; Kim, G.; Koo Lee, Y. E.; Hah, H. J.; Ethirajan, M.; Pandey, R. K.; Kopelman, R. Multifunctional biodegradable polyacrylamide nanocarriers for cancer theranostics—A "see and treat" strategy. *ACS Nano* **2012**, *6*, 6843−6851.
(25) Bardhan, R.; Lal, S.; Joshi, A.; Halas, N. J. Theranostic Nanoshells: From Probe Design to Imaging and Treatment of Cancer. *Acc. Chem. Res.* **2011**, *44*, 936−946.
(26) Mieszawska, A. J.; Mulder, W. J. M.; Fayad, Z. A.; Cormode, D. P. Multifunctional Gold Nanoparticles for Diagnosis and Therapy of Disease. *Mol. Pharmaceutics* **2013**, *10*, 831−84.
(27) Santra, S.; Kaittanis, C.; Santiesteban, O. J.; Perez, J. M. Cell-specific, activatable, and theranostic prodrug for dual-targeted cancer imaging and therapy. *J. Am. Chem. Soc.* **2011**, *133*, 16680−16688.
(28) Fan, Z.; Shelton, M.; Singh, A. K.; Senapati, D.; Khan, S. A.; Ray, P. C. Multifunctional Plasmonic Shell−Magnetic Core Nanoparticles for Targeted Diagnostics, Isolation, and Photothermal Destruction of Tumor Cells. *ACS Nano* **2012**, *6*, 1075−1083.
(29) Schuller, J. A.; Barnard, E. S.; Cai, W.; Jun, Y. C.; White, J. S.; Brongersma, M. L. Plasmonics for extreme light concentration and manipulation. *Nat. Mater.* **2010**, *9*, 193−204.
(30) Lu, W.; Singh, A. K.; Khan, S. A.; Senapati, D.; Yu, H.; Ray, P. C. Gold Nano-Popcorn Based Targeted Diagonosis, Nanotherapy Treatment and In-Situ Monitoring of Photothermal Therapy Response of Prostate Cancer Cells Using Surface Enhanced Raman Spectroscopy. *J. Am. Chem. Soc.* **2010**, *132*, 18103−18114.
(31) Duncan, R.; Gaspar, R. Nanomedicine(s) under the Microscope. *Mol. Pharmaceutics* **2011**, *8*, 2101−2141.
(32) Singh, A. K.; Khan, S. A.; Fan, Z.; Demeritte, T.; Senapati, D.; Kanchanapally, R.; Ray, P. C. Development of a Long-Range Surface-Enhanced Raman Spectroscopy Ruler. *J. Am. Chem. Soc.* **2012**, *134*, 8662−8669.
(33) Huang, X.; El-Sayed, I. H.; Qian, W.; El-Sayed, M. A. Cancer Cell Imaging and Photothermal Therapy in the Near-Infrared Region by Using Gold Nanorods. *J. Am. Chem. Soc.* **2006**, 2115−2120.
(34) Lu, W.; Arumugam, S. R.; Senapati, D.; Singh, A. K.; Arbneshi, T.; Khan, S. A.; Yu, H.; Ray, P. C. Multifunctional Oval Shape Gold Nanoparticle Based Selective Detection of Breast Cancer Cells Using Simple Colorimetric and Highly Sensitive Two-Photon Scattering Assay. *ACS Nano* **2010**, *4*, 1739−1749.
(35) Huschka, R.; Neumann, O.; Barhoumi, A.; Halas, N. J. Visualizing light-triggered release of molecules inside living cells. *Nano Lett.* **2010**, *10*, 4117−4122.
(36) Wang, E.; Desai, M. S.; Lee, S. K. Light-Controlled Graphene-Elastin Composite Hydrogel Actuators. *Nano Lett.* **2013**, *13*, 2826−2830.
(37) Fan, Z.; Senapati, D.; Singh, A. K.; Ray, P. C. Theranostic Magnetic Core−Plasmonic Shell Star Shape Nanoparticle for the Isolation of Targeted Rare Tumor Cells from Whole Blood, Fluorescence Imaging, and Photothermal Destruction of Cancer. *Mol. Pharmaceutics* **2013**, *10*, 857−866.
(38) Yuan, H.; Fales, A. M.; Vo-Dinh, T. TAT Peptide-Functionalized Gold Nanostars: Enhanced Intracellular Delivery and Efficient NIR photothermal therapy Using Ultralow Irradiance. *J. Am. Chem. Soc.* **2012**, *134*, 11358−11361.
(39) Davis, M. E. The first targeted delivery of siRNA in humans via a self-assembling, cyclodextrin polymer-based nanoparticle: from concept to clinic. *Mol. Pharmaceutics* **2009**, *6*, 659−668.
(40) Sardana, G.; Jung, K.; Stephan, C.; Diamandis, E. P. Proteomic analysis of conditioned media from the PC3, LNCaP, and 22Rv1 prostate cancer cell lines: discovery and validation of candidate prostate cancer biomarkers. *J. Proteome Res.* **2008**, *7*, 3329−3338.
(41) Ray, P. C.; Khan, S. A.; Singh, A. K.; Senapati, D.; Fan, Z. Nanomaterial for Targeted Detection and Photothermal Killing of Bacteria. *Chem. Soc. Rev.* **2012**, *41*, 3193−3209.
(42) Song, J.; Zhou, J.; Duan, H. Self-Assembled Plasmonic Vesicles of SERS-Encoded Amphiphilic Gold Nanoparticles for Cancer Cell Targeting and Traceable Intracellular Drug Delivery. *J. Am. Chem. Soc.* **2012**, *134*, 13458−13469.
(43) Liu, X.; Dai, Q.; Austin, L.; Coutts, J.; Knowles, G.; Zou, J.; Chen, H.; Huo, Q. A One-Step Homogeneous Immunoassay for Cancer Biomarker Detection Using Gold Nanoparticle Probes Coupled with Dynamic Light Scattering. *J. Am. Chem. Soc.* **2008**, *130*, 2780−2782.
(44) Thomas, C. R.; Ferris, D. P.; Lee, J. H.; Choi, E.; Cho, M. H.; Kim, E. S.; Stoddart, J. F.; Shin, J. S.; Cheon, J.; Zink, J. I. Noninvasive Remote-Controlled Release of Drug Molecules in Vitro Using Magnetic Actuation of Mechanized Nanoparticles. *J. Am. Chem. Soc.* **2010**, *132*, 10623−10625.
(45) Beqa, L.; Fan, Z.; Singh, A. K.; Senapati, D.; Ray, P. C. Gold Nano-Popcorn Attached SWCNT Hybrid Nanomaterial for Targeted Diagnosis and Photothermal Therapy of Human Breast Cancer Cells. *ACS Appl. Mater. Interfaces* **2011**, *3*, 3316−3324.
(46) Noimark, S.; Dunnill, C. W.; Kay, W. M. C.; Perni., S.; Prokopovich, P.; Ismail, S.; Wilson, M.; Parkin, I. V. Incorporation of methylene blue and nanogold into polyvinyl chloride catheters; a new approach for light-activated disinfection of surfaces. *J. Mater. Chem.* **2012**, *22*, 15388−15396.
(47) Usacheva, M. N.; Teichert, M. C.; Biel, M. A. The role of the methylene blue and toluidine blue monomers and dimers in the photoinactivation of bacteria. *J. Photochem. Photobiol. B* **2003**, *71*, 87−98.
(48) Tang, W.; Xu, H.; Park, E. J.; Philbert, M. A.; Kopelman, R. Encapsulation of methylene blue in polyacrylamide nanoparticle platforms protects its photodynamic effectiveness. *Biochem. Biophys. Res. Commun.* **2008**, *369*, 579−83.
(49) Tada, D. B.; Vono, L. L. R.; Duarte, E. L.; Itri, R.; Kiyohara, P. K.; Baptista, M. S.; Rossi, L. M. Methylene Blue-Containing Silica-Coated Magnetic Particles: A Potential Magnetic Carrier for Photodynamic Therapy. *Langmuir* **2007**, *23*, 8194−8199.